# *MICROMACHINED STIMULATING ELECTRODES*

## Quarterly Report #5

(Contract NIH-NINDS-N01-NS-2-2379)

October --- December 1993

Submitted to the

***Neural Prosthesis Program***
National Institute of Neurological Disorders and Stroke
National Institutes of Health

by the

*Solid-State Electronics Laboratory*
*Bioelectrical Sciences Laboratory*
Department of Electrical Engineering and Computer Science
University of Michigan
Ann Arbor, Michigan
48109-2122

February 1994

# *MICROMACHINED STIMULATING ELECTRODES*

## *Summary*

During the past quarter, research under this program has gone forward in a number of areas. Fabrication runs of "EMORY" and "HMRI" probes have been completed successfully and additional wafers of both mask sets are in process. These probes include both recording and stimulating designs and have gold pads with either gold or iridium sites. Recently-deposited iridium appears normal and has not exhibited the adhesion problems that were symptomatic of other recent runs. Penetration probes have been completed which will allow penetration force through pia arachnoid and dura mater to be quantified as a function of microscopic tip shape. Three different tip processes have been used: deep boron-diffused, double-diffused with a shallow boron diffusion to define the tip, and a chisel tip structure formed by combining a deep boron diffusion with a reactive ion etch (RIE) step. For each tip process, probes have been formed having a variety of tip angles (10° - 45°) and different numbers of shanks. The probes are equipped with electrodes to allow recording and stimulation as well as piezoresistive strain gauges to allow a direct readout of the force on the shank during insertion. The penetration studies will begin during the coming term.

Chronic experiments in two adult guinea pigs were performed during the past term to better understand the impedance of iridium electrodes in such situations. Three-shank six-site passive probes were used with two 1000$\mu m^2$ iridium sites per shank. The stimulation waveform was a biphasic (charge-balanced, cathodic-first) pulse 100$\mu$s per phase in length at a frequency of 500Hz. The current amplitude was 50$\mu$A. The impedances of these sites remained roughly constant throughout the week of stimulation for all four electrode site pairs tested. We have also performed additional finite element simulations to better understand the effects of site size on the ability of sites to inject high current/charge levels into tissue. Simulations show relatively high current densities near the edges of stimulation sites compared with the densities near their centers but also show that these edge current densities are reduced for multiple closely-spaced sites. As site area is decreased, a greater portion of the site area appears to be close enough to the edges that the overall current density over the electrode is increased, reducing the dependence of electrode current capacity on the site area. This has also been observed experimentally.

Efforts to realize active stimulating probes containing on-chip signal processing circuitry are continuing. Test samples using 0.46$\mu$m of LTO dielectric above the circuit area were unsuccessful during the past term due to a small incidence of pinholes around contact vias. This is being corrected by increasing the LTO to the 1.2$\mu$m thickness used previously. Completed active probes are expected during the coming term.

# *MICROMACHINED STIMULATING ELECTRODES*

## *1. Introduction*

The goal of this research is the development of active multichannel arrays of stimulating electrodes suitable for studies of neural information processing at the cellular level and for a variety of closed-loop neural prostheses. The probes should be able to enter neural tissue with minimal disturbance to the neural networks there and deliver highly-controlled (spatially and temporally) charge waveforms to the tissue on a chronic basis. The probes consist of several thin-film conductors supported on a micromachined silicon substrate and insulated from it and from the surrounding electrolyte by silicon dioxide and silicon nitride dielectric films. The stimulating sites are activated iridium, defined photolithographically using a lift-off process. Passive probes having a variety of site sizes and shank configurations have been fabricated successfully and distributed to a number of research organizations nationally for evaluation in many different research preparations. For chronic use, the biggest problem associated with these passive probes concerns their leads, which must interface the probe to the outside world. Even using silicon-substrate ribbon cables, the number of allowable interconnects is necessarily limited, and yet a great many stimulating sites are ultimately desirable in order to achieve high spatial localization of the stimulus currents.

The integration of signal processing electronics on the rear of the probe substrate (creating an "active" probe) allows the use of serial digital input data which can be demultiplexed onto the probe to provide access to a large number of stimulating sites. Our goal in this area of the program has been to develop a family of active probes capable of chronic implantation in tissue. For such probes, the digital input data must be translated on the probe into per-channel current amplitudes which are then applied to the tissue through the sites. Such probes require five external leads, virtually independent of the number of sites used. As discussed in our previous reports, we are now developing a series of three active probes containing CMOS signal processing electronics. Two of these probes are slightly redesigned versions of an earlier first-generation set of designs and are designated as STIM-1A and STIM-1B. The third probe, STIM-2, is a second-generation version of our high-end first-generation design, STIM-1. All three probes provide 8-bit resolution in setting the per-channel current amplitudes. STIM-1A and -1B offer a biphasic range from 0μA to ±254μA with a resolution of 2μA, while STIM-2 has a range from 0 to ±127μA with a resolution of 1μA. STIM-2 offers the ability to select 8 of 64 electrode sites and to drive these sites independently and in parallel, while -1A allows only 2 of 16 sites to be active at a time (bipolar operation). STIM-1B is a monopolar probe, which allows the user to guide an externally-provided current to any one of 16 sites as selected by the digital input address. The high-end STIM-2 contains provisions for numerous saftey checks and for features such as remote impedance testing in addition to its normal operating modes. It also offers the option of being able to record from any one of the selected sites in addition to stimulation.

During the past quarter, research on this contract has focused in several areas. Probes continue to be fabricated for external users and distributed to them for use in their research programs. Recent runs with iridium stimulating sites have not exhibited the adhesion problems seen previously. We have now completed the first samples of

penetration probes, aimed at quantifying the insertion force required for penetration of membranes such as pia arachnoid and dura mater as a function of the microscopic tip shape. In addition, we have conducted chronic stimulation experiments in two animals aimed at examining site impedances over time in chronic situations. Additional finite-element simulations have also been conducted to better understand the effects of site size and nonuniform current distributions on the current/charge delivery capability of such sites. Efforts at completing the first samples of chronic stimulating probes are continuing but have been delayed during part of the past quarter by delays in obtaining satisfactory LTO coatings to protect the circuit areas during final silicon etch. Working probes are expected during the coming quarter.

## 2. *Passive Stimulating Electrode Development*

During the past quarter, additional process runs of probes from the "EMORY" and "HMRI" mask sets were performed successfully. These probes are discussed in a companion report on our recording contract and will not be discussed further here. It is important to note, however, that these probes were fabricated with iridium sites and gold bonding pads and that the iridium sites appear normal in all respects. No adhesion problems are in evidence, and the impedance levels on unactivated sites are in the same range as earlier probes that have performed well, both in activation and in-vivo. In addition, we have completed the first runs on probes for penetration studies and on 3D platform assemblies during the past quarter. These devices are described below.

### 2.1 *Penetration Studies*

As discussed in previous quarterly reports, a series of probes have been designed to study the insertion forces, long-term probe-tissue coupling, and tissue damage associated with penetration through the pia arachnoid and dura mater in guinea pigs, rats and perhaps primates. These probes will be used to determine the optimum probe tip geometry which allows for ease of penetration with minimal cortical surface dimpling, minimal tissue damage and reaction along the insertion track, and maximum tissue-electrode coupling.

During the past quarter, processing of several wafers of penetration probes was completed, each wafer representing a different tip configuration: 1) a blunt tip formed using a deep boron diffusion , 2) a sharp tip formed using a shallow boron diffusion, and 3) an attempt at a quasi-chisel tip utilizing a vertical Reactive Ion Etch (RIE). As mentioned in previous quarterly reports, all three of these tip configurations are implemented on an entire set of probes having different tip angles and shank configurations. Except for the process variations noted above for each wafer, the three configurations use the same mask set and fabrication process. Figure 1 shows a scanning electron microscope (SEM) picture of a probe with a 65μm-wide shank (drawn mask width) and a 10° shallow boron-diffused tip. The four-point-probe electrode configuration on this probe can also be seen with two stimulation sites flanking two recording sites. The four-point-probe will be used to test tissue resistivity along the shank to measure the size of the tissue fluid pool that collects along it, both acutely and in chronic situations. In contrast, Fig. 2 shows a probe with a 65μm wide shank featuring a 45° deep boron-diffused tip. These two tips demonstrate the opposite ends of the spectrum as far as tip sharpness is concerned. Figure 3 demonstrates a probe with a 65μm wide shank and a 45° tip angle that is half way between a deep boron-diffused tip and a quasi-chisel tip. It is actually a quasi-chisel tip on which the final RIE step did not go deep enough to cut through all of the lateral boron diffusion area. While not actually a finished probe, it does

illustrate the effectiveness of the RIE in forming a sharp tip. A longer RIE will be used in the probes used in penetration studies to complete formation of this chisel tip structure.

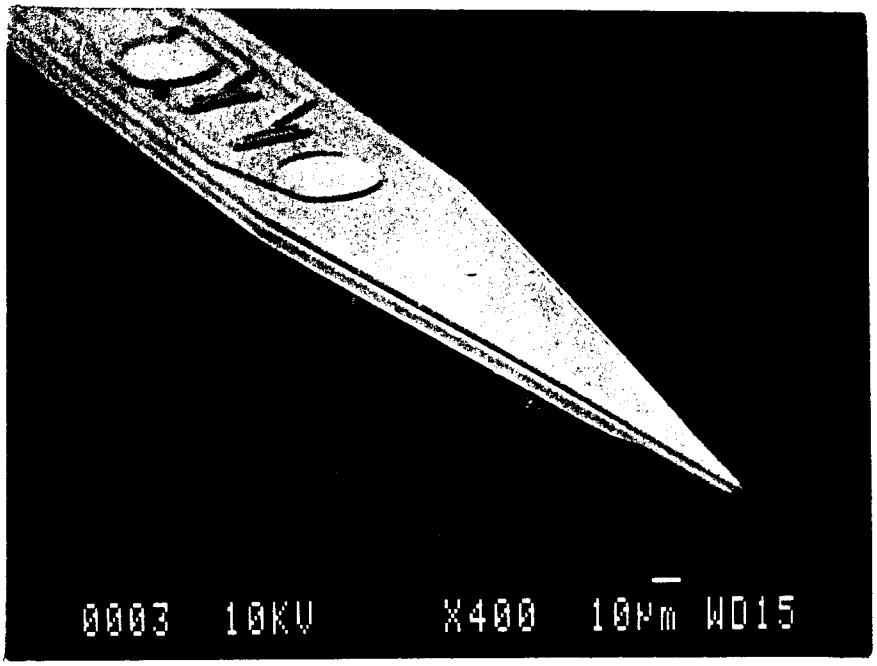


Fig. 1: A 65µm-wide probe shank (drawn mask width) with a 10° shallow boron-diffused tip. The four-point-probe electrode configuration is also visible.

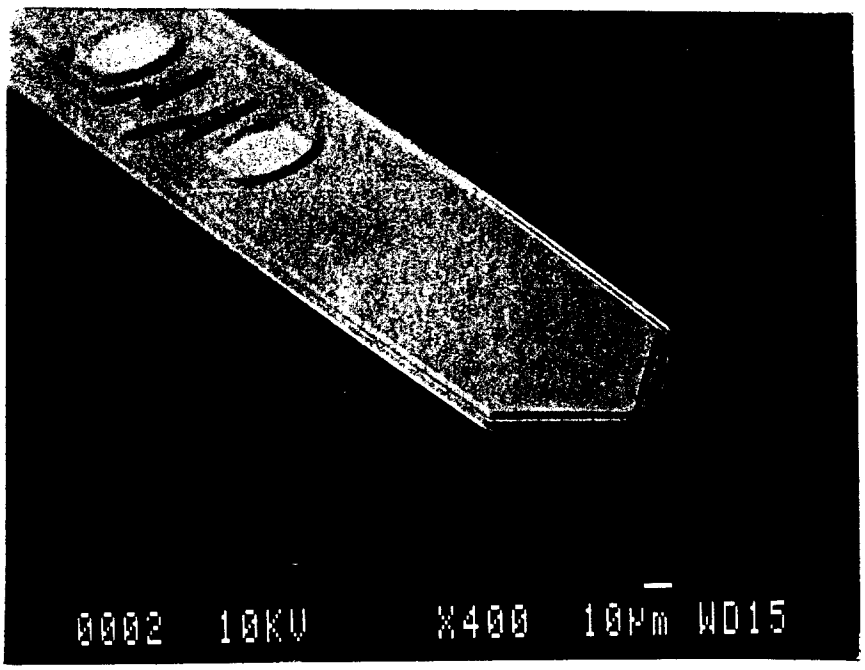


Fig. 2: A 65µm wide probe shank (drawn mask width) with a 45° deep boron-diffused tip. The four-point-probe electrode configuration is also visible.

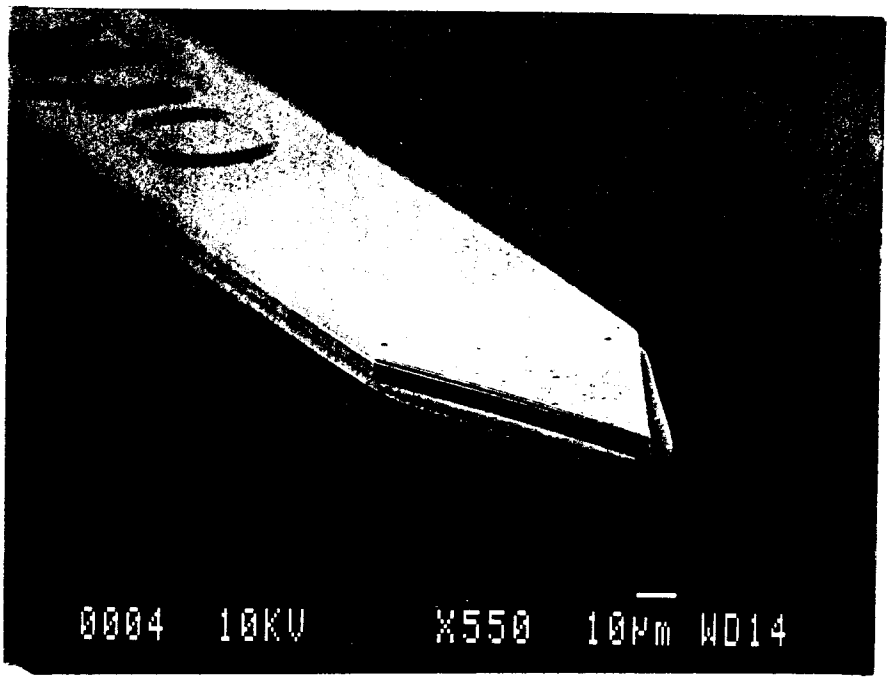


Fig. 3: A 65µm-wide probe shank (drawn mask width) with a 45° reactive-ion-etched chisel tip partially etched through the deep boron diffusion defining the shank. The four-point-probe electrode configuration is also visible.

Close-ups of these three different tip configurations are shown in Figs. 4-6, illustrating more clearly the differences among the shallow boron-diffused tip, the deep boron-diffused tip, and the RIE-etched chisel tip, all at the same magnification. In Fig. 4, showing the shallow boron-diffused tip, it is apparent that the thickness of the dielectric layers is comparable to the thickness of the shallow boron-diffused tip. If this study reveals that sharp tips are the best in terms of achieving penetration with minimum force, it would be beneficial to terminate the dielectric layers short of the actual silicon tip in order to further reduce the tip size. This would cause the tissue to see approximately a 1µm step as the probe tip penetrates.

A very high magnification photograph of a 10° shallow boron-diffused tip is shown in Fig. 7. This picture gives a good perspective as to the true size of the tip when compared to the 1µm scale line. Figure 7 also reveals a very slight gap between the dielectric layers and the boron-doped silicon underlying them along the edges of the dielectric. This is believed to be the result of the boron segregation from the underlying silicon into the oxide during high temperature oxide growth. The slight reduction in boron doping level at the surface allows some etching of the silicon by EDP during the final silicon etch step to separate the probes from the wafer. The separation is probably very limited in lateral extent and is unlikely to cause any problems, but it is worthy of extra attention in these tip fabrication and penetration studies.

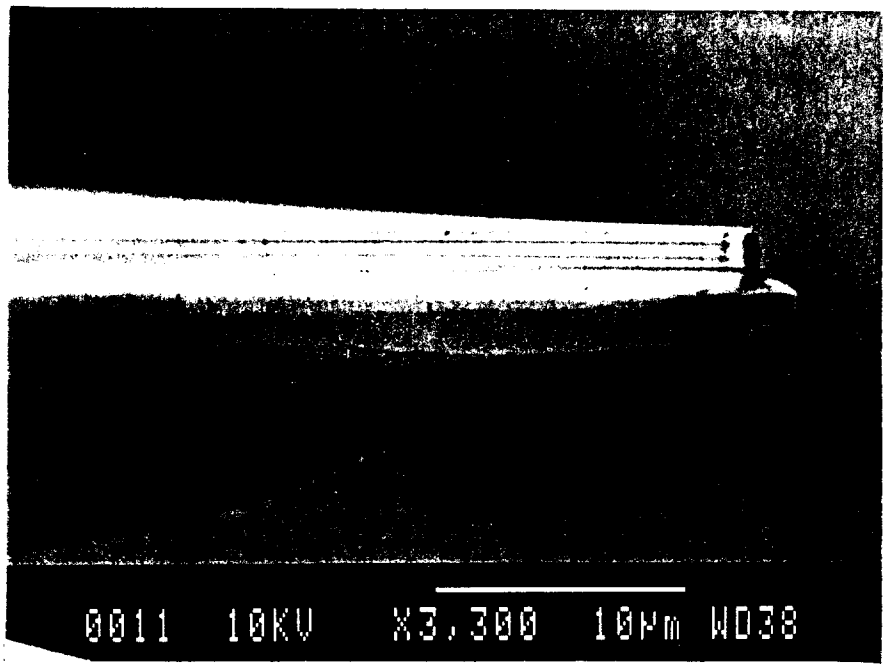


Fig. 4: A close-up of a 65µm-wide probe shank (drawn mask width) with a 10° shallow boron-diffused tip.

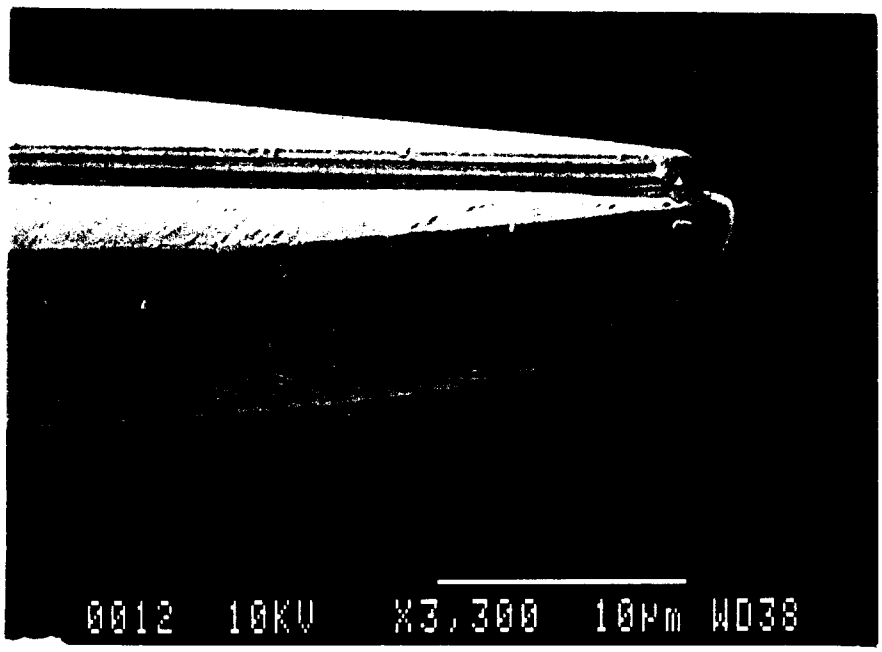


Fig. 5: A close-up of a 65µm wide probe shank (drawn mask width) with a 10° deep boron-diffused tip.

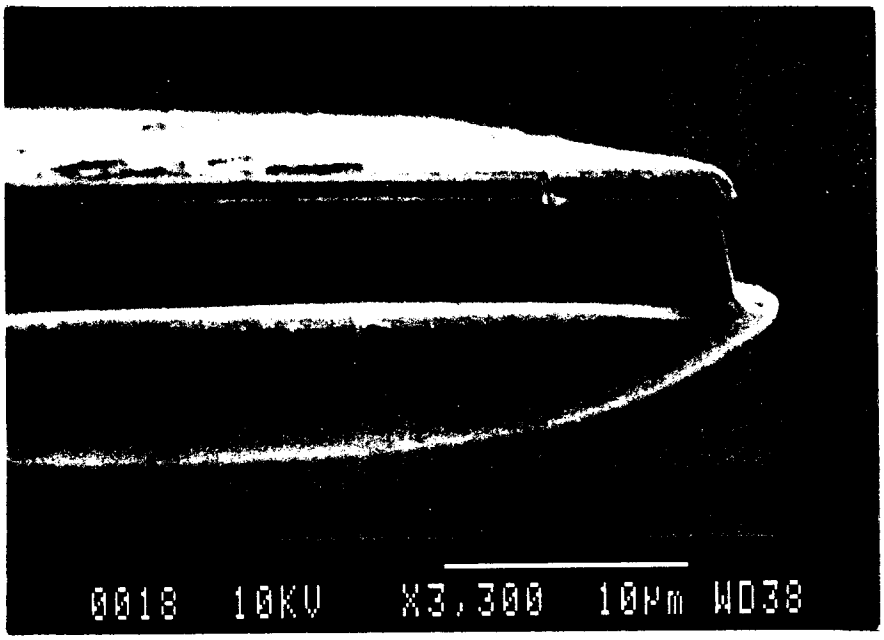


Fig. 6: A close-up of a 65µm wide probe shank (drawn mask width) with a 45° RIE-etched chisel edge etched partially through the deep boron diffusion defining the tip.

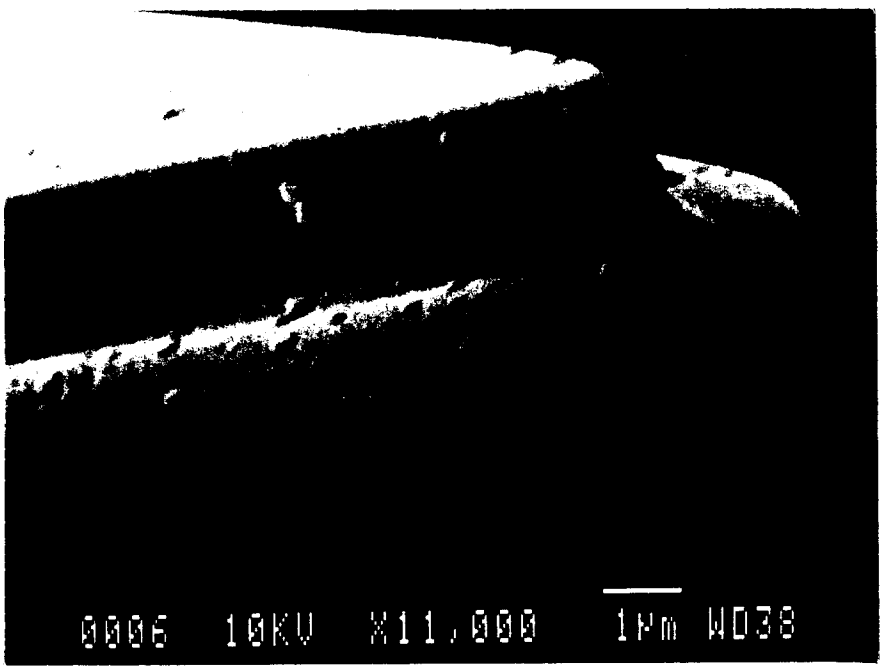


Fig. 7: An SEM view of the tip of a 10° shallow boron-diffused tip. The oxide-nitride-oxide-nitride-oxide dielectric sequence is clearly visible.

A photo of one of the chronic probes included for this study is shown in Fig. 8. The probe is to be used for chronic studies of tissue resistivity, which may lend insight into the size and time-course of the fluid pool surrounding a probe after insertion due to injury. This is only expected to be used over the course of days or at most weeks, since the wound will heal, and the fluid will be re-absorbed by the tissue. An important feature of this probe is its very low support area on the back of the shank (200μm high). This is expected to reduce the problem of the probe back area fusing to the cranium as the wound heals. The 90° exit of the double-strand periodically cross-bridged ribbon cable is also very important. This allows the cable to exit through a slit in the dura mater a distance from the actual probe site which should also help reduce scar tissue fusion to the back end of the probe. If the cable fuses to the wound it will still allow freedom of probe movement as long as the cable is not taut. Freedom of probe movement is felt to be important so that the probe can 'float' with pulsation and movement of the brain surface. The double-stranded cable is important in that it allows for a wider cable area without compromising flexibility. It also helps to minimize cross-talk between the stimulating and recording leads because they are actually on different strands of the cable. There are periodic cross-bridges linking the two strands as one cable for handling purposes.

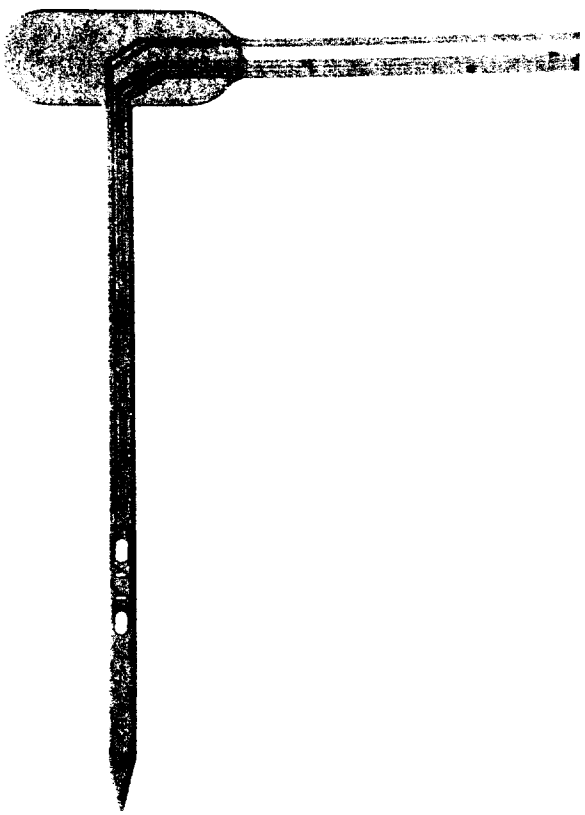

Fig. 8: A chronic tissue resistivity probe with a 90° double-stranded cross-bridged ribbon cable.

The iridium sites on these penetration probes appear to be normal and of high quality. Previously, we have had intermittant but sometimes serious iridium adhesion problems. We have come to believe that this may be a problem with contamination of our sputtering machine by other materials that are sputtered in the same machine. In order to try to eliminate any contamination-induced loss of adhesion, two sputtering runs were performed before actually sputtering the probe wafers. This was done to try to cover any contaminants in the sputtering chamber with iridium. Inspection of the wafers revealed no peeling of the iridium from the electrodes, and scratch tests using a diamond stylus appeared normal. Subsequent to EDP, no loss of adhesion has been observed in the finished probes either. Impedance tests of probes from this fabrication run revealed normal magnitude and phase characteristics.

Though calibration of the polysilicon strain gauges included on the probes for penetration force measurements is not yet complete, they are fully functional and demonstrate a variation in resistance of about ±100 ohms at maximum deflection around a stress-free resistance value of approximately 1750 ohms. This sensitivity appears to be quite adequate for the intended study. We hope to automate the calibration process using a computer-controlled microdrive to place known deflections on the probes while measuring the associated changes in resistance. This will require pushing the tip of the probe against something rigid. Assuming this does not cause damage to the probe tips, it should be very easy to calibrate each probe before it is used. If any tip damage is noted, we will settle for calibrating several representative probes and will assume the probes used in penetration studies will perform similarly.

Now that we have most of the necessary probes fabricated and the data acquisition system is nearing readiness with the recent purchase of a National Instruments I/O board, we expect to be able to move into the experiment stage soon. We anticipate completing the acute penetration studies during the next quarter as well as the implantation of probes for chronic studies.

## *2.2 In-Vivo Current Flow and Impedance Studies*

Experiments have been run with passive stimulating electrodes during the past quarter. Two chronic guinea pig implants were tested over a period of one week each. The impedance of the probe tissue system remained at the same order-of-magnitude level throughout the week for all four electrode site pairs tested. This result contradicts findings reported in the last quarter. Also, a trend of increasing impedance during stimulation was noted. The details of the experiments are discussed below.

The experiment has been described at length in previous reports and will only be reviewed briefly here. An adult guinea pig is implanted with a three-shank six-site passive probe. There are two 1000$\mu m^2$ iridium sites per shank. To increase charge delivery capacity and decrease impedance, the sites are activated before implantation. The probe is placed in the right visual cortex. The animal is allowed to recover for 7-10 days, after which it under goes five straight days of stimulation. Current is passed through two different site pairs for four hours each. One site pair consists of sites on different shanks (i.e., between shanks) and the other site pair is on the same shank (along shank). The stimulation waveform is a biphasic pulse of pulse length 100$\mu s$ per phase and frequency 500Hz. The stimulation current level is 50$\mu A$. Impedance and access voltage data is taken before, during, and after the experiment. Stimulus generation and data acquisition is

handled by a 486PC running LabVIEW (National Instruments). The results are analyzed with MATLAB.

The above experiment was carried out with two guinea pigs. The site-to-site impedance data for these experiments are given in Charts 1-4 below. These measurements must be viewed in terms of the original impedance of the probe in-vitro. These numbers are given below in Table 1.

*Site to Site Impedance Data for Four Site Pairs in Two Animals*

Chart 1: Animal #1, Along Shank Stimulation

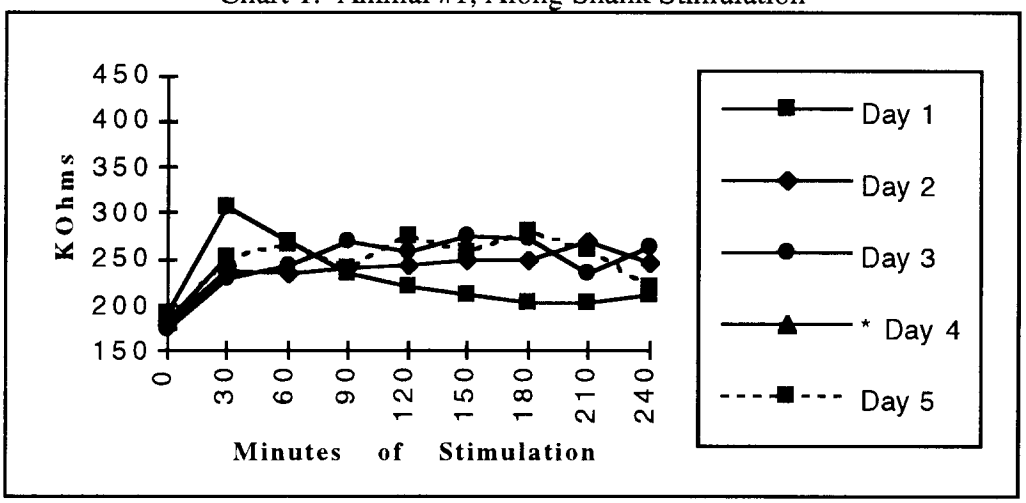


Chart 2: Animal #1, Between Shank Stimulation

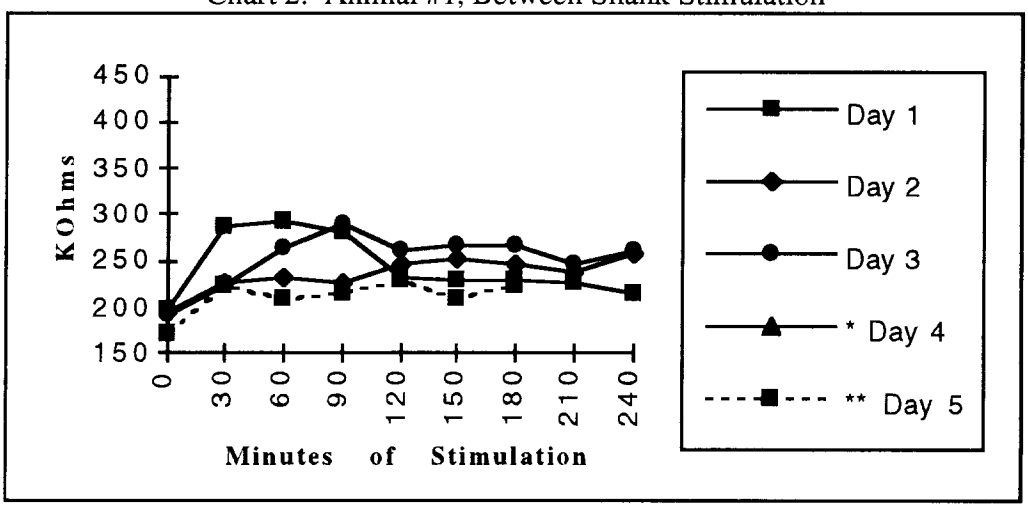

Chart 3: Animal #2, Along Shank Stimulation

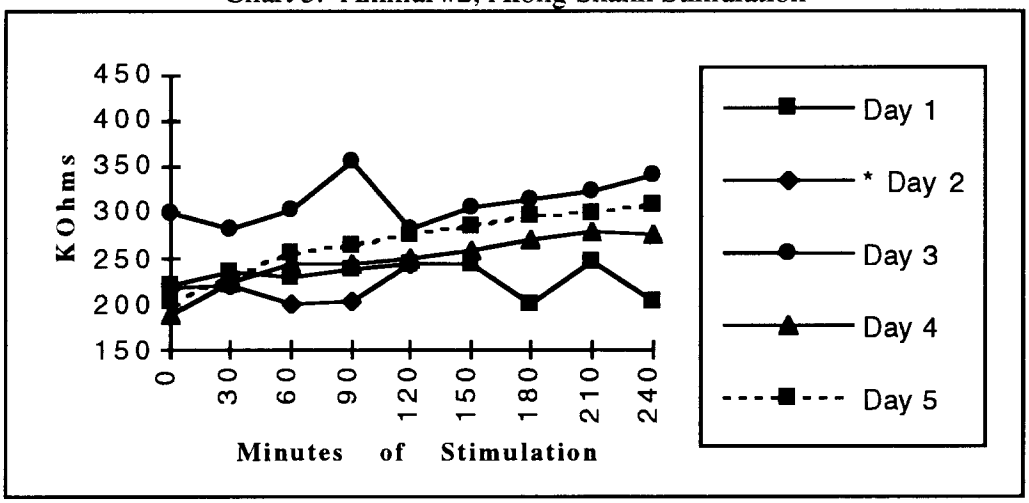


Chart 4: Animal#2, Between Shank Stimulation

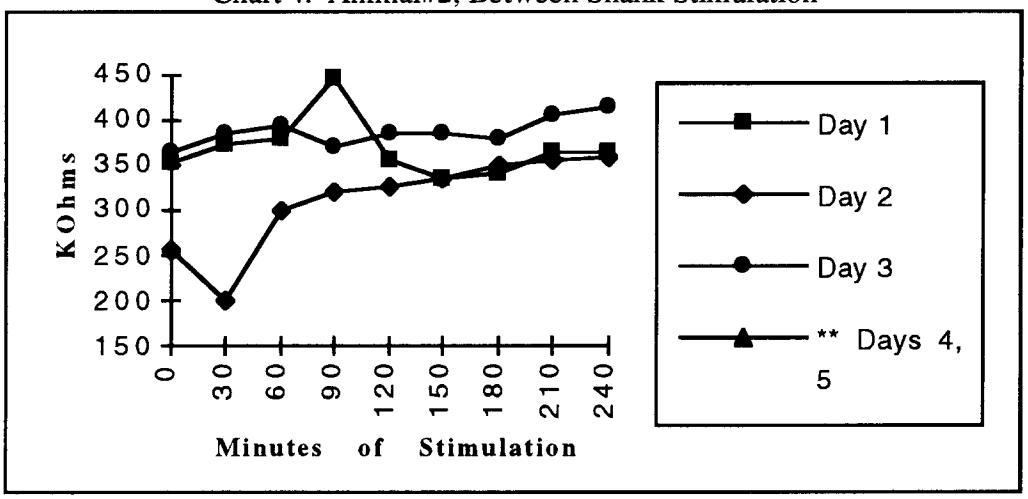


* - Data missing as a result of equipment malfunction
** - Data missing as a result of electrode failure

Table 1: Site-to-Site Impedance of Electrode Sites In-Vitro (in K-Ohms)

| | |
|---|---|
| Animal 1, Along Shank | 180 |
| Animal 1, Between Shanks | 100 |
| Animal 2, Along Shank | 120 |
| Animal 2, Between Shanks | 300 |

In animal #1, along-shank impedance rises only slightly after implantation while between-shank impedance almost doubles. In animal #2, the impedance *in-vivo* is significantly higher for both site pairs. These levels are maintained throughout the experiment. In the last report, an experiment was discussed which indicated a large drop in impedance during the week of the test. That result was viewed as questionable then. In light of these latest findings, that initial result can probably be attributed to some kind of probe or connector failure. In both experiments, one general trend was evident. The impedances rose during the stimulation period, only to return to a lower level by the start of the next day. It is not clear whether this impedance change is taking place in the electrode or the tissue. Regardless, the present impedance level is unacceptably high. Passing 50μA through these probes develops an access voltage of 10-15V.

During the next quarter we hope to accomplish several tasks that will help us understand the above results. Further testing will be conducted, including more chronic implants and running the experiment *in vitro*. A more detailed analysis of the access voltage records will be done to try and determine which voltages are attributable to electrode impedance and which to tissue impedance. Histological results showing tissue reaction may show a correlation between probe encapsulation and measured parameters. Electrodes with different site sizes and activation levels will be implanted to study the effects of these parameters on access voltage. In the more distant future, this data will be helpful in the development of a model of current flow through tissue.

## *2.3 Modeling and Simulation of Stimulating Sites*

During the past several years, we have developed planar iridium oxide stimulating electrodes and have characterized their mechanical and electrical behavior as a function of deposition (sputtering) conditions. Parameters of interest have included internal film stress, adhesion, charge capacity, and maximum charge delivery. Based on these experimental results, we have demonstrated patterned and double-sided electrode structures for small-site applications and the use of multiple parallel electrodes ("waffle electrodes") for large stimulating sites. In this report, we will discuss additional efforts to understand the electrical characteristics of these electrodes and the effects of site size through finite-element simulations.

The use of many small electrodes in place of one large site has been shown to produce improved electrical characteristics (higher current capability, or longer operating life at the same overall stimulating current level) due to the much larger peripheral area of such multi-site structures. Figure 9 shows two simple site structures and the normalized electric field surrounding the site as a function of normalized site position. For these simulations, a fixed drive potential is assumed and the electric field lines in the solution are calculated. These field lines then set the initial current density distribution over the site. For the case of two sites, the spacing between sites has been assumed equal to the site width. This simulation illustrates the significantly greater field (and current) concentration along the edges of the site and the relatively low field present near the center. Such distributions have been well known. It is noted that using the finite-element approach, it is straightforward to show the effects, for example, of recessed electrode edges on the resulting current density. The maximum current density along the electrode edges sets the operating limits on the site since this density must stay below the metallic corrosion limit for the electrode surface as well as below the tissue damage limit. The electrode potential excursion must also stay within the water window to avoid gas evolution. Figure 9 shows

that the great majority of the current is carried by the outer 20-30 percent of the electrode width. It also suggests that for multiple sites, the current density at the center is slightly higher and the current density at the edges is slightly less than for a single isolated electrode. The use of multiple sites in a "waffle" configuration is intuitively correct to increase the current handling capability since it results in greatly increased "edge" area, allowing a greater portion of the electrode surface to operate at the higher current densities found there.

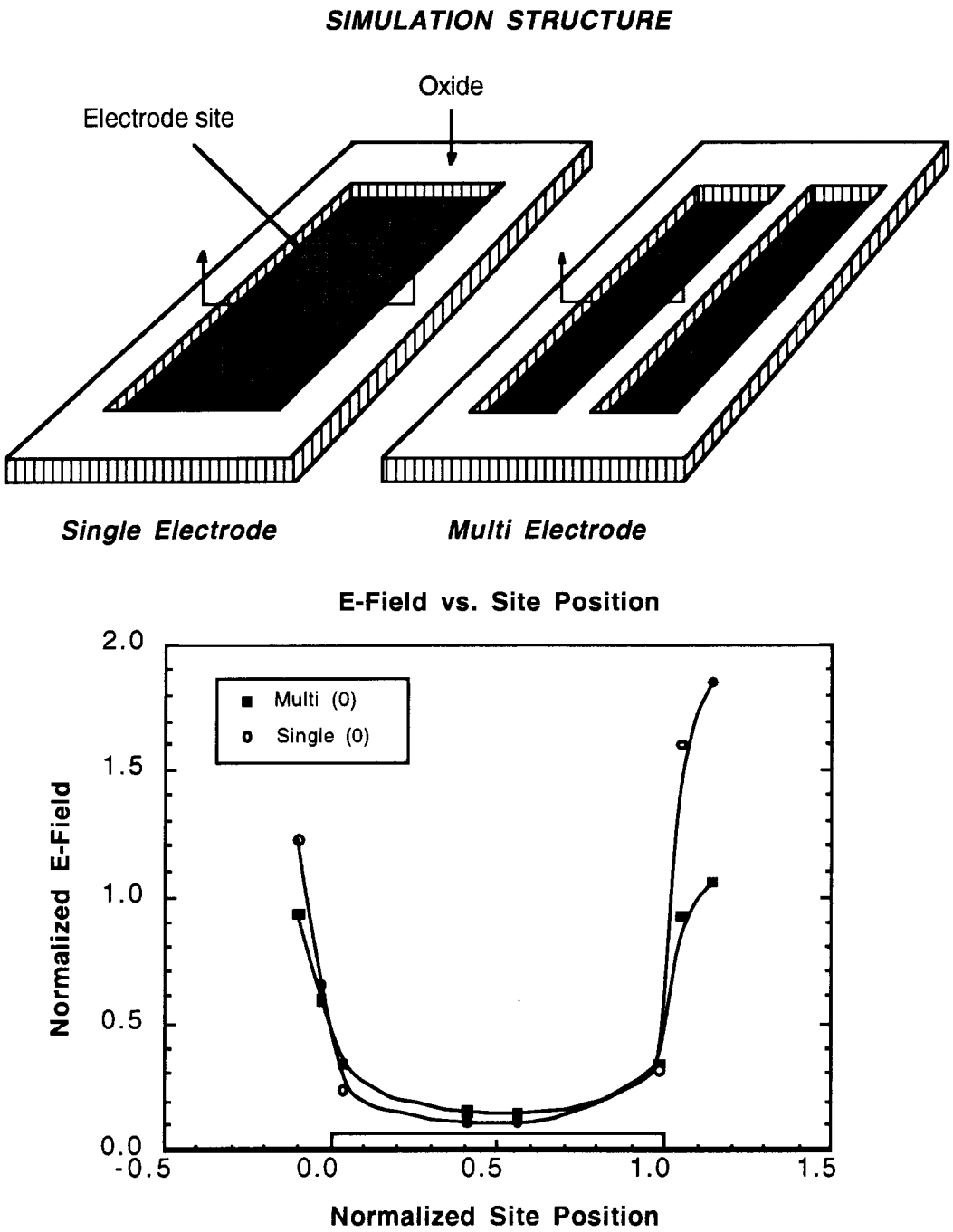


Fig. 9: Simulation site structures and the normalized field distribution as a function of normalized site position for a single and multiple electrodes.

Figure 10 shows the conceptual electric field distributions around single and multiple sites. As a large single site is divided into many smaller sites, the electric field near the internal site edges is reduced and smoothed, but the average field (and resulting average current density) is substantially higher than for a single site alone. The rather sharp electric field along the edge region is modified by interactions with the fields from adjacent electrodes so that a flattening effect at the edges is evident. This effect becomes more significant as the distance between sites decreases.

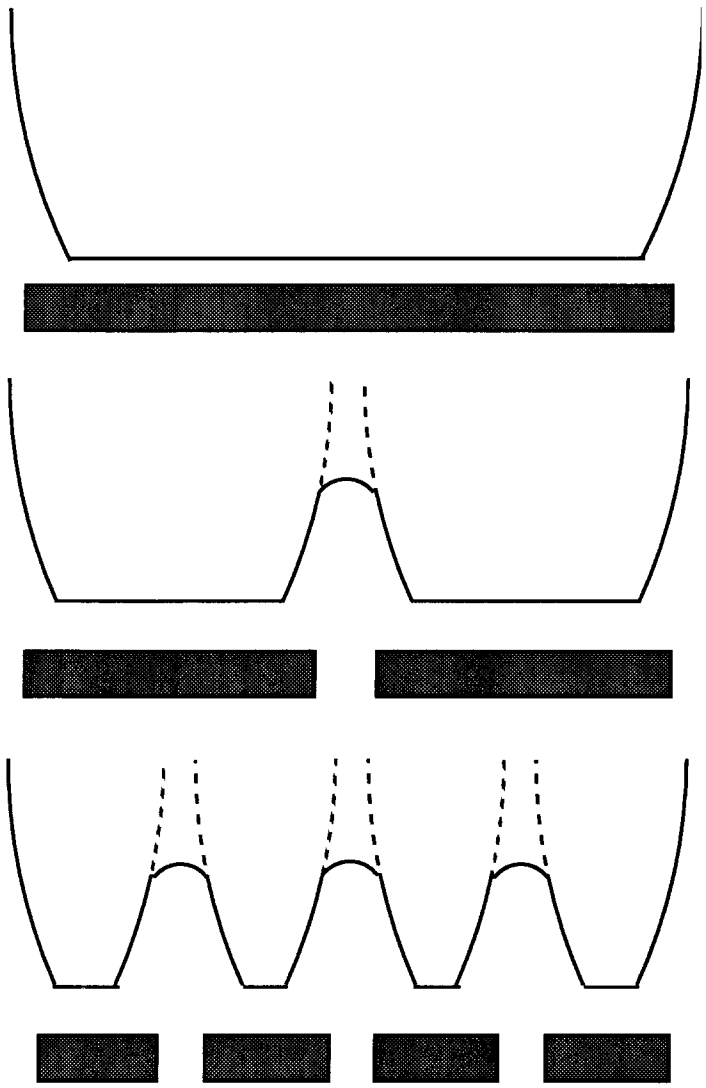

Fig. 10: Conceptual electric field distribution for single and multiple sites.

Figure 11 shows the simulated field distributions for different site sizes, and Fig. 12 shows the normalized electric field at the center and edge of the sites. As site size decreases, the average electric field intensities also increase slightly, increasing the current density over the site. More importantly, however, the "edge" region occupies a larger portion of the total electrode area for a smaller site, increasing the current capability of the site at a given maximum field.

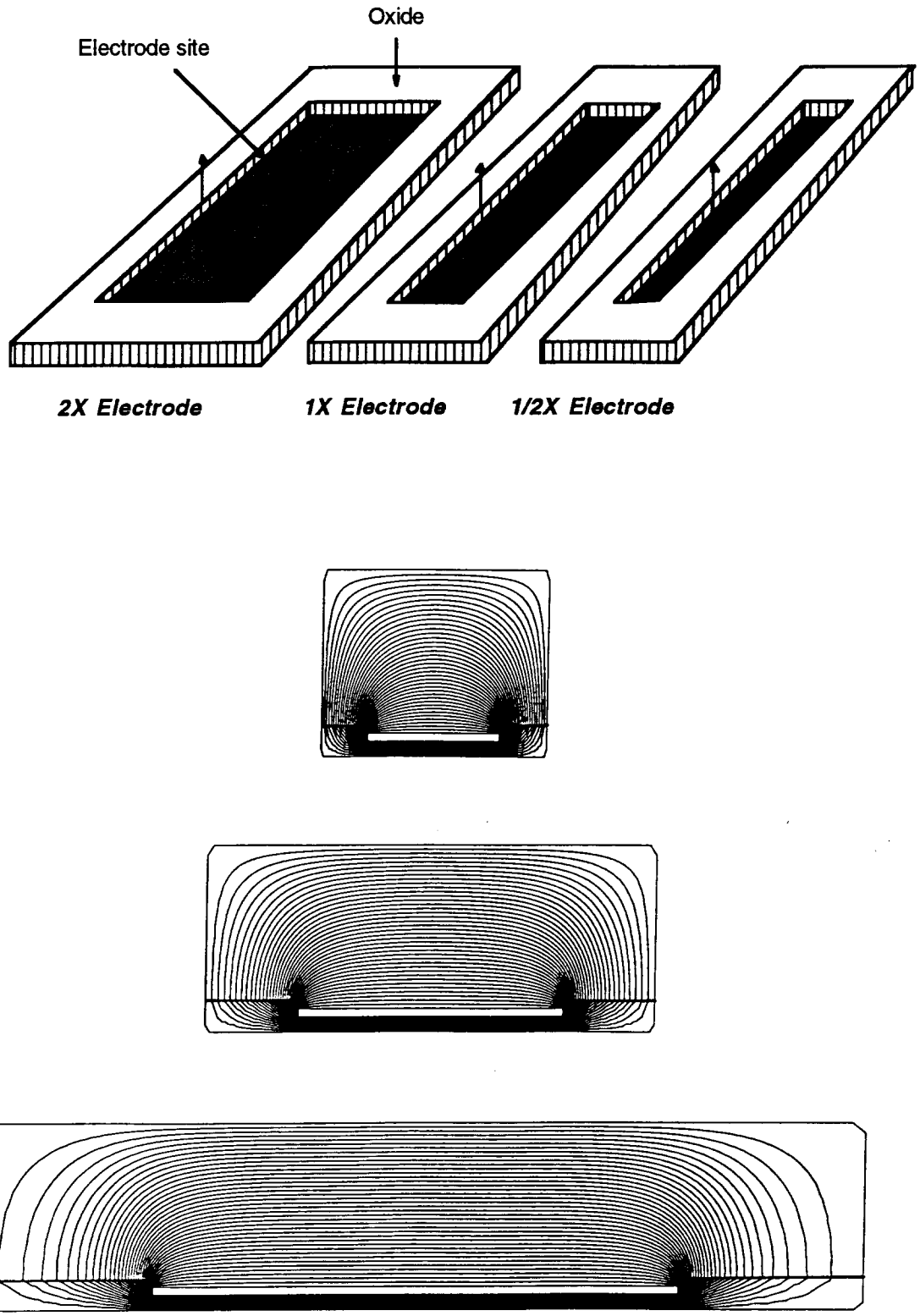


Fig. 11: Site structures and their electric field distributions for different site sizes.

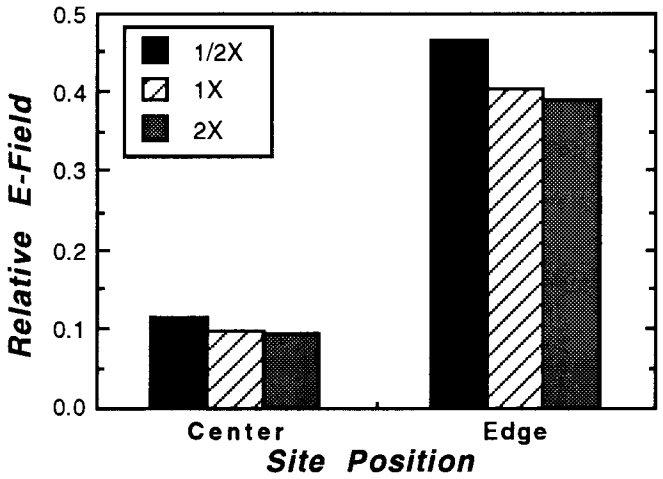


Fig. 12: Relative electric field distributions at the center and edges of a site for various site sizes.

If one assumes that the center and edge fields above are at least approximately correct, then as long as the field distribution profile over the site does not vary with site size the current density over the site should also be roughly independent of site dimension and site area. To investigate the behavior of the maximum deliverable charge capability of an electrode as a function of its site area, several planar sites having areas from 100$\mu m^2$ to 4000$\mu m^2$ were prepared and activated in CBS solution between the voltage limits of -0.9 and +1.2$V_{SCE}$ at a sweep rate of 2.1V/sec for 25min. The electrodes were then stimulated with cathodic-first, biphasic, 200$\mu$sec pulses at 100Hz, and $Q_{Dmax}$ was measured by increasing the current amplitudes until the potential on the electrode (with iR drops subtracted) reached the negative or positive voltage limits set by the operational water window ($\pm$1$V_{SCE}$ in this test). The charge per phase being delivered at that point was measured and is plotted in Fig. 13. As can be seen, the maximum deliverable charge density ($Q_{D,\,max}$) increases significantly experimentally as the site area decreases. Such increases have been observed previously by us and by others. Hence, we expect that as the site size decreases, edge currents become much more significant as a function of the total current, effectively increasing the current/charge density. Simulations are being carried out to confirm this observation. As the site area decreases, however, the associated increase in access resistance and IR tissue drop makes sites less than 1000$\mu m^2$ in size increasingly less attractive, particularly for sites containing on-chip electronics.

## *3. Development of Active Stimulating Probes (STIM-2)*

During the past quarter, two problems delayed the completion of our second-generation active stimulation probes. The first was a relatively long delay in having low-temperature oxide (LTO) deposited for us by industry, and the second involved the physical separation of our iridium sputtering target reported previously. We are moving toward installation of our own LTO system, which will solve the first problem during the coming year. The iridium target has now been fixed and a backup target ordered, solving the second problem as well.

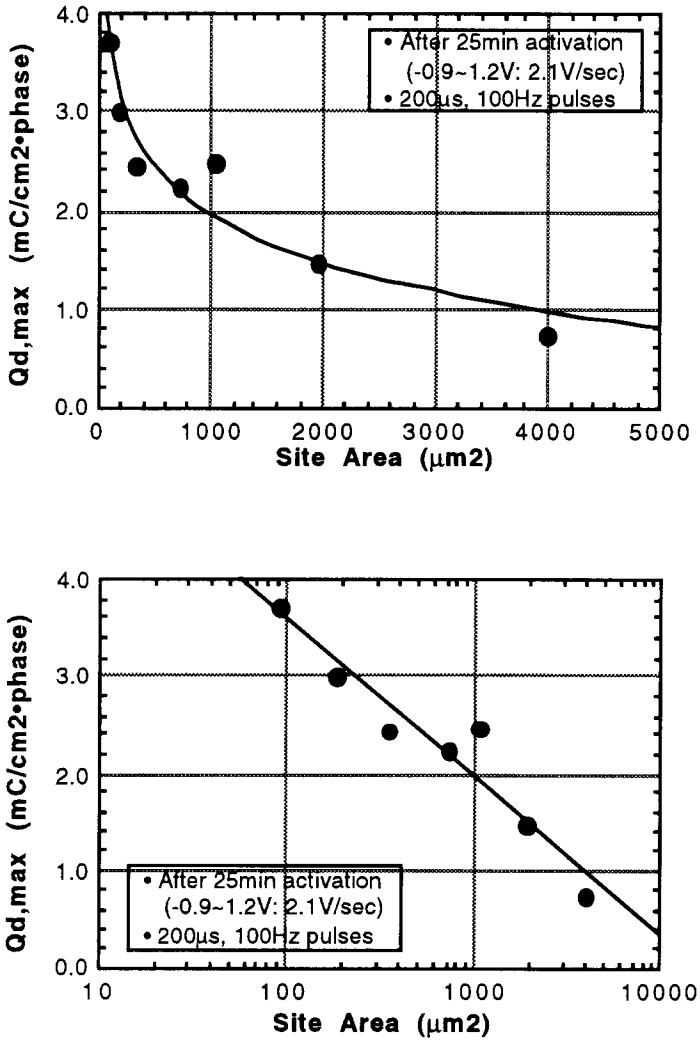


Fig. 13: Maximum deliverable charge density measured for 200µs-duration charge-balanced CF current pulses for various iridium oxide site areas. Linear plot (above) and logarithmic plot (below).

Toward the end of the quarter, wafers were deposited with a layer of LTO 0.46µm thick. This is thinner than the 1.2µm previously used, but was felt to be thick enough for passivation purposes, and the decreased time at the 400°C deposition temperature should ensure minimal threshold shifts during this operation. The LTO etch rate in EDP is only 25nm/hour compared with about 80µm/hour for lightly-doped silicon. However, two problems were encountered during the final die separation etch on a test wafer fun with this LTO thickness. The first involved attack of some of the contacts in EDP as shown in Fig. 14. The problem was restricted to only a small percentage of contacts on the wafer, but any attack whatsoever is intolerable. Close inspection revealed a step coverage problem at this thickness, less severe than that encountered with PECVD films but nonetheless sufficient at a few contacts to allow the etch to get to the underlying silicon. The remaining wafers will be coated with an additional 0.7µm of LTO and possibly will be capped using a gold inlay over the active circuitry to avoid this problem.

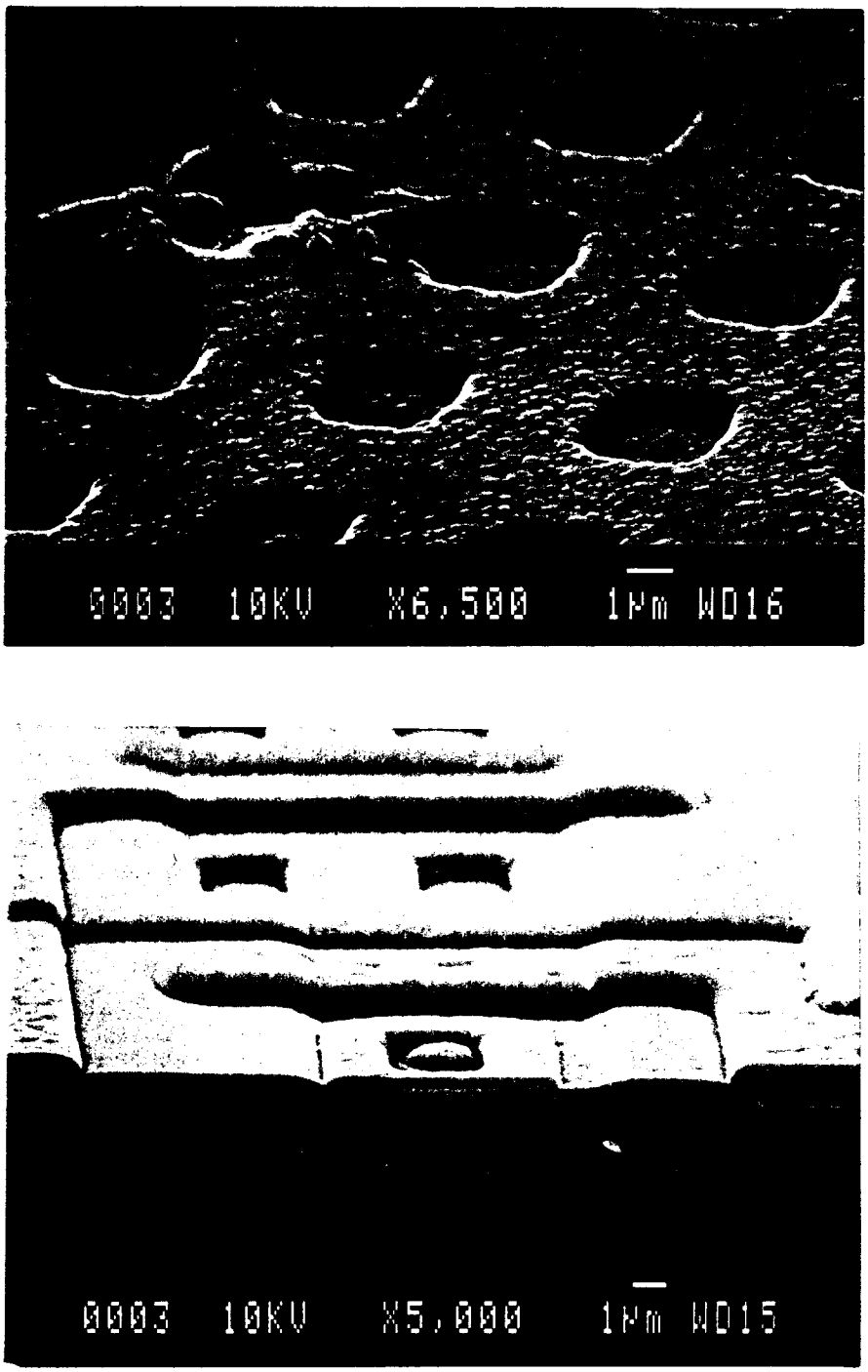


Fig. 14: SEM photographs showing attack of contacts on an active probe circuitry after 2 hours of EDP etching. In this test, a 0.46μm-thick layer of LTO was deposited for the protection of CMOS contacts and circuitry.

The second problem involved the etching difficulties mentioned in the previous report. If the circuitry is not oriented slightly off the major wafer flat (these wafers were not), then with straight shanks there is no undercutting of either cables or shanks from the front of the wafer (except at the shank tips, where the undercut is slow compared with the shank length). Thus, it is difficult to form the shanks and the thin cables while simultaneously preserving a thicker area under the circuitry. This problem can easily be solved by slightly misaligning the wafers with respect to the major flat so that undercutting of the narrow shanks and cables from the front does occur or by using an electrochemical etch-stop to halt the etch over the circuit area. Thus, while annoying on the present run, the problem has known solutions that do not complicate the overall process. Figure 15 shows the tip of a STIM-2 shank and a representative site.

During the coming term, the present group of active stimulating probes will be completed and tested in-vitro. If results are positive, we will proceed to in-vivo testing as well.

## *4. Conclusions*

During the past quarter, research under this program has gone forward in a number of areas. Fabrication runs of "EMORY" and "HMRI" probes have been completed successfully and additional wafers of both mask sets are in process. These probes include both recording and stimulating designs and have gold pads with either gold or iridium sites. Recently-deposited iridium appears normal and has not exhibited the adhesion problems that were symptomatic of other recent runs. Penetration probes have been completed which will allow penetration force through pia arachnoid and dura mater to be quantified as a function of microscopic tip shape. Three different tip processes have been used: deep boron-diffused, double-diffused with a shallow boron diffusion to define the tip, and a chisel tip structure formed by combining a deep boron diffusion with a reactive ion etch (RIE) step. For each tip process, probes have been formed having a variety of tip angles (10° - 45°) and different numbers of shanks. The probes are equipped with electrodes to allow recording and stimulation as well as piezoresistive strain gauges to allow a direct readout of the force on the shank during insertion. The penetration studies will begin during the coming term.

Chronic experiments in two adult guinea pigs were performed during the past term to better understand the impedance of iridium electrodes in such situations. Three-shank six-site passive probes were used with two 1000$\mu m^2$ iridium sites per shank. The stimulation waveform was a biphasic (charge-balanced, cathodic-first) pulse 100$\mu$s per phase in length at a frequency of 500Hz. The current amplitude was 50$\mu$A. The impedances of these sites remained roughly constant throughout the week of stimulation for all four electrode site pairs tested. We have also performed additional finite element simulations to better understand the effects of site size on the ability of sites to inject high current/charge levels into tissue. Simulations show relatively high current densities near the edges of stimulation sites compared with the densities near their centers but also show that these edge current densities are reduced for multiple closely-spaced sites. As site area is decreased, a greater portion of the area appears to be close enough to the edges that the overall current density over the electrode is increased, reducing the dependence of electrode current capacity on the site area. This has also been observed experimentally.

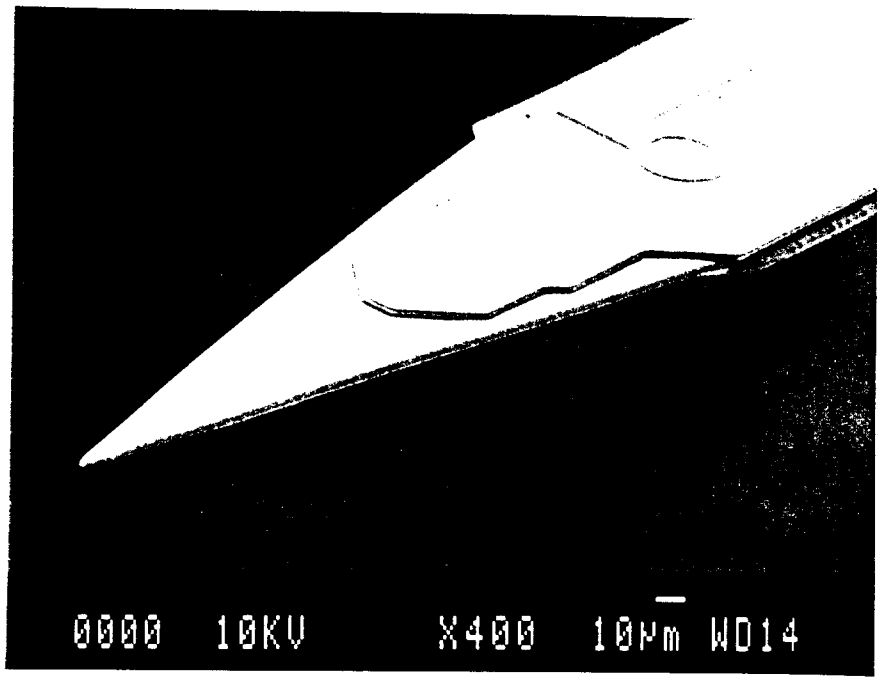


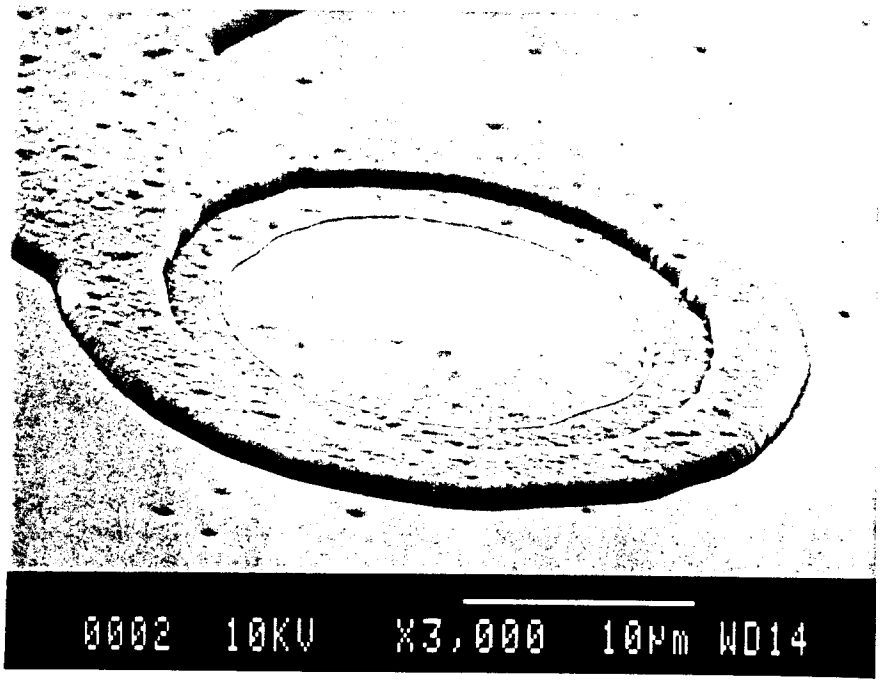


Fig. 15: SEM photographs of the tip of one of the current active probes with high-temperature LPCVD dielectrics and LTO in place over the shanks. A stimulating site is shown below. LTO is removed over a broader area around the site, leaving the iridium inlayed into an opening in the LPCVD dielectrics. Small irregularities in the site shape emphasize the use, and importance, of a self-aligned site process.

Efforts to realize active stimulating probes containing on-chip signal processing circuitry are continuing. Test samples using 0.46μm of LTO dielectric above the circuit area were unsuccessful during the past term due to a small incidence of pinholes around contact vias. This is being corrected by increasing the LTO to the 1.2μm thickness used previously. Completed active probes are expected during the coming term.